



Contents lists available at ScienceDirect

## Journal of Sound and Vibration

journal homepage: [www.elsevier.com/locate/jsvi](http://www.elsevier.com/locate/jsvi)

# Nonlinear effects of flow unsteadiness on the acoustic radiation of a heaving airfoil



Avshalom Manela\*

Faculty of Aerospace Engineering, Technion - Israel Institute of Technology, Haifa 32000, Israel

## ARTICLE INFO

## Article history:

Received 4 August 2012

Received in revised form

17 June 2013

Accepted 19 August 2013

Handling Editor: D. Juve

Available online 14 September 2013

## ABSTRACT

The study considers the combined effects of boundary animation (small-amplitude heaving) and incoming flow unsteadiness (incident vorticity) on the vibroacoustic signature of a thin rigid airfoil in low-Mach number flow. The potential-flow problem is analysed using the Brown and Michael equation, yielding the incident vortex trajectory and time evolution of trailing edge wake. The dynamical description serves as an effective source term to evaluate the far-field sound using Powell–Howe analogy. The results identify the fluid–airfoil system as a dipole-type source, and demonstrate the significance of nonlinear eddy–airfoil interactions on the acoustic radiation. Based on the value of scaled heaving frequency  $\omega a/U$  (with  $\omega$  the dimensional heaving frequency,  $a$  the airfoil half-chord, and  $U$  the mean flow speed), the system behaviour can be divided into two characteristic regimes: (i) for  $\omega a/U \ll 1$ , the effect of heaving is minor, and the acoustic response is well approximated by considering the interaction of a line vortex with a stationary airfoil; (ii) for  $\omega a/U \gg 1$ , the impact of heaving is dominant, radiating sound through an “airfoil motion” dipole oriented along the direction of heaving. In between (for  $\omega a/U \sim O(1)$ ), an intermediate regime takes place. The results indicate that trailing edge vorticity has a two-fold impact on the acoustic far field: while reducing pressure fluctuations generated by incident vortex interaction with the airfoil, trailing edge vortices transmit sound along the mean-flow direction, characterized by airfoil heaving frequency. The “silencing” effect of trailing edge vorticity is particularly efficient when the incident vortex passes close to the airfoil trailing edge: at that time, application of the Kutta condition implies the release of a trailing edge vortex in the opposite direction to the incident vortex; the released vortex then detaches from the airfoil and follows the incident vortex, forming a “silent” vortex pair. By analysing the nonlinear fluid–structure interaction problem, the present work aims at complementing existing studies, in which linear eddy–airfoil interactions are considered for unforced configurations.

© 2013 Elsevier Ltd. All rights reserved.

## 1. Introduction

The coupling between dynamics of thin structures and ambient fluid flow is a classical problem in fluid–structure interactions which has attracted considerable attention over the years [1–3]. Specific interest in the associated vibroacoustic problem has evolved owing to its relevance to engineering applications and biological phenomena. These include, among others, the generation of palatal snoring sound [4]; the coupling between acoustic disturbances and aerodynamic

\* Tel.: +972 48292237; fax: +972 48292030.

E-mail address: [amanela@technion.ac.il](mailto:amanela@technion.ac.il)

performance of micro-air-vehicle wings [5]; and the design of flapping-based active noise control systems for the reduction of blade-vortex interaction noise [6,7]. Strong coupling between thin-structure actuation and flow unsteadiness is also common during insect flight, where typical small thickness-to-chord wing ratios are encountered [8]. These motions result in the radiation of a wide variety of noises known as “insect songs” [9,10], which are important factors in the social and sexual behaviour of various insect species (e.g., [11]). Consequently, several works have studied the sound field of insect-wing configurations, both experimentally [12] and numerically [13].

Existing studies on the motion and acoustic signature of thin airfoils in unsteady flows have considered various aspects of the problem. In the context of the dynamical problem, Manela and Howe [14] studied the unforced fluid–structure interaction between a flexible filament and uniform flow, while Alben [15] and Michelin and Llewellyn Smith [16] examined the small-amplitude motion of an elastic appendage actuated at its leading edge. The counterpart acoustic problem was studied by Manela [17], who considered the vibroacoustic response of an elastic plate to arbitrary (small-amplitude) non-periodic boundary actuation.

A separate set of works focused on the effect of incoming flow unsteadiness on the motion and sound of *unforced* fluid–structure configurations. Incoming flow unsteadiness was modelled by a single or a sequence of line vortices interacting with the structure. Howe [18] analysed the generation of sound by a single vortex convected past a rigid stationary airfoil. In later contributions, a semi-infinite geometry was considered and elastic degrees of freedom were added to the structure [19,20]. Manela and Howe [21] studied the motion of an elastic flag induced by a street of vortices released from its pole. More recently, the acoustic radiation of a flexible plate interacting with a rectilinear line vortex was studied [22].

All Refs. [18–22] have focused on a linearized setup where the incident vortex strength is small and the structure is unforced by external (other than ambient fluid) loads. In such a setup, the vortex convects along a straight line with the mean uniform flow, unaffected by the image vorticity induced by the structure. These assumptions were partially relaxed by Abou-Hussein et al. [23], who examined the effect of nonlinear vortex–structure interaction on the trajectory and acoustic radiation of a line vortex passing above a stationary rigid plate, with no direct account taken of the evolution of trailing edge wake. Tang and co-workers [24–26] have then applied a similar approach to analyse the effect of elasticity on vortex sound emitted in other unforced configurations of practical importance.

The objective of the present work is to analyse the *combined* effects of flow unsteadiness (incident vorticity) and boundary animation on the acoustic radiation of a thin airfoil. Such conditions are common in flapping flight, where the wing is actively actuated and interacts with unsteady gust or incoming turbulence. For simplicity, we consider a two-dimensional setup of a thin rigid airfoil actuated by periodic heaving motion and affecting the motion of an incident line vortex passing in its vicinity. After analysing the dynamical problem, we apply the Powell–Howe acoustic analogy [2,27] (valid in the present low-Mach and high-Reynolds number setup) to evaluate the far-field sound. By considering this setup we seek to examine the basic nonlinear coupling mechanism between boundary actuation and vortex sound.

The remaining parts of the paper are organized as follows: in Sections 2 and 3 the fluid dynamical and acoustic problems are formulated, respectively. Numerical results are presented and discussed in Section 4. A summary of the main findings of the work and concluding comments are given in Section 5.

## 2. Dynamical problem

Consider a two-dimensional thin rigid airfoil of length  $2a$  subject to low-Mach high-Reynolds number flow of velocity  $\mathbf{U} = U\hat{\mathbf{x}}_1$ , parallel to the airfoil chord (Fig. 1). The airfoil is located between  $-a \leq x_1 \leq a$  and displaced periodically at time  $t \geq 0$  in the  $x_2$ -direction with prescribed small-amplitude heaving motion,

$$\xi(t \geq 0) = \bar{\epsilon}a \cos \omega t, \quad (1)$$

where  $\bar{\epsilon} \ll 1$  and  $\omega$  denotes the heaving frequency. An incident line vortex of strength  $\Gamma$  is released into the flow at a given location at time  $t=0$  and moves within the vicinity of the airfoil. In what follows we analyse the near-field fluid motion and far-field acoustic radiation of the fluid–airfoil system.

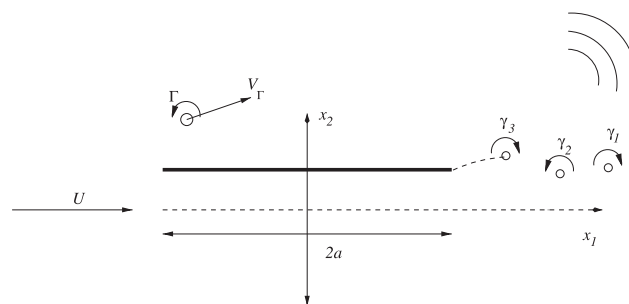


**Fig. 1.** Schematic of the problem. A thin rigid airfoil of length  $2a$  is set in small-amplitude periodic heaving motion in the  $x_2$ -direction. The airfoil is subject to uniform low-Mach stream at speed  $U$  in the  $x_1$ -direction and to a line vortex of strength  $\Gamma$  in the spanwise direction.

To analyse the acoustic radiation of the system, particular care should be given to the modelling of fluid vorticity. In the present potential-flow setup, fluid vorticity is concentrated at the incident vortex location and along a trailing edge wake. Vorticity may also be released at the airfoil leading edge, where flow separation may occur. However, in the present level of approximation, and following existing theoretical investigations of flows around actuated thin structures [15–17], we neglect any flow separation upstream of the trailing edge, and allow the flow velocity and pressure to diverge as the inverse square root of distance from the leading edge. This divergence results in a finite leading-edge “suction” force on the airfoil, which is an acceptable model for the force in actual flow [28], and serves as a standard model for describing flows past slender airfoils [29]. We further discuss the impact of this approximation on the calculated acoustic field in Section 5.

### 2.1. Flow complex potential

We consider an initial value problem where at time  $t=0$  the incident vortex  $\Gamma$  is set into the flow and the airfoil starts heaving. The instantaneous vortex location and velocity at time  $t$  are denoted by  $\mathbf{x}_\Gamma(t)$  and  $\mathbf{v}_\Gamma(t) = d\mathbf{x}_\Gamma/dt$ , respectively. Setting  $z = x_1 + ix_2$ , the flow complex potential is given by the superposition

$$w(z, t) = (w_\Gamma + w_\xi + w_\gamma)H(t) + Uz, \quad (2)$$

representing the separate contributions of incident vortex ( $w_\Gamma$ ), plate motion ( $w_\xi$ ), trailing edge wake ( $w_\gamma$ ), and uniform flow ( $Uz$ ). Here  $H(t)$  is the heaviside step function, imposing initial conditions of a stationary plate and no incoming flow unsteadiness at time  $t < 0$ .

The potential  $w_\Gamma$  is obtained by mapping the fluid region in the  $z$ -plane into the region outside the unit circle in the  $\zeta$ -plane, using the time-dependent Joukowski-type transformation

$$\zeta(s) = \frac{s(z, t)}{a} + \sqrt{\frac{(s(z, t))^2}{a^2} - 1}, \quad s(z, t) = z - i\xi(t). \quad (3)$$

Using (3), the airfoil is mapped into a stationary strip ( $|\operatorname{Re}\{s\}| \leq a$ ,  $\operatorname{Im}\{s\} = 0$ ) in the  $s$ -plane, and the vortex location is mapped into  $\zeta_\Gamma = \zeta(z_\Gamma)$  in the  $\zeta$ -plane. To satisfy the impermeability condition on the unit circle  $|\zeta| = 1$ , we place an image vortex  $-\Gamma$  at the inverse point  $\zeta = 1/\zeta_\Gamma^*$  (with an asterisk denoting the complex conjugate of a complex number), together with a vortex  $\Gamma$  at the centre of the circle, ensuring that the total circulation around the cylinder vanishes at time  $t=0$ . This yields

$$w_\Gamma(\zeta) = -\frac{i\Gamma}{2\pi} \ln(\zeta - \zeta_\Gamma) + \frac{i\Gamma}{2\pi} \ln\left(\zeta - \frac{1}{\zeta_\Gamma^*}\right) - \frac{i\Gamma}{2\pi} \ln \zeta. \quad (4)$$

Similarly, using the transformation (3), the potential  $w_\xi$  induced by the plate motion normal to itself is

$$w_\xi(\zeta) = -iv_n a / \zeta, \quad (5)$$

where  $v_n = d\xi/dt$  marks the instantaneous airfoil velocity, calculated from (1).

The fluid velocities derived from (4) and (5) exhibit square-root singularities at the airfoil leading and trailing edges. To obtain finite velocity at the trailing edge, the unsteady Kutta condition should be imposed. This necessitates release of vorticity from the airfoil trailing edge into a trailing edge wake, which we now turn to analyse.

### 2.2. Evolution of trailing edge wake

Previous theoretical approximations of high Reynolds number vortex shedding from two-dimensional airfoils have been frequently based on the Brown and Michael equation [30,31], originally suggested for the evaluation of lift on delta wings. According to this model, the shedding of vorticity is discretized as a set of line vortices whose position and strength vary with time. At a given time instant, one vortex is being shed from the airfoil trailing edge, in the form of a thin connecting sheet of infinitesimal circulation which ends in a concentrated core of finite circulation. Denoting the core circulation by  $\gamma_n$ , Fig. 1 illustrates schematically the case  $n=3$ , where the thin connecting sheet is marked by the dashed line connecting the trailing edge and  $\gamma_3$ . The core strength changes with time according to the Kutta condition, while its position  $\mathbf{x}_{\gamma_n}$  is governed by the Brown and Michael formula (see (6)). When the time derivative  $d\gamma_n/dt$  changes sign, the vortex is detached from the thin sheet and propagates as a “free” line vortex with “frozen” (fixed) circulation. At the same time, shedding of a new vortex ( $\gamma_{n+1}$ ) is initiated.

Howe [32] reappraised the Brown and Michael equation by accounting for inconsistent surface forces introduced by the original formulation. A rigorous procedure has led to an *emended* form of the equation

$$\frac{d\mathbf{x}_{\gamma_n}}{dt} \cdot \nabla \Psi_i + \frac{\Psi_i}{\gamma_n} \frac{d\gamma_n}{dt} = \mathbf{v}_{\gamma_n} \cdot \nabla \Psi_i, \quad (6)$$

which will be applied hereby. Here  $\Psi_i(\mathbf{x}, t)$  ( $i=1,2$ ) is the stream function corresponding to a flow of unit speed in the  $i$ -direction at large distances from the airfoil surface, and  $\mathbf{v}_{\gamma_n}$  is the velocity at  $\gamma_n$  with its local self-potential excluded. For the present case of a thin flat airfoil stationary in the  $s$ -plane,

$$\Psi_1 = \operatorname{Im}\{s\} \quad \text{and} \quad \Psi_2 = \operatorname{Im}\left\{-i\sqrt{s^2 - a^2}\right\}. \quad (7)$$

Substituting (7) into (6) yields the complex form of the Brown and Michael equation in our setup:

$$\frac{ds_{\gamma_n}^*}{dt} + \left( s_{\gamma_n}^* \frac{\operatorname{Re}\{a^2 \sqrt{s_{\gamma_n}^2 - a^2}\}}{\operatorname{Re}\{s_{\gamma_n}^* \sqrt{s_{\gamma_n}^2 - a^2}\}} \right) \frac{1}{\gamma_n} \frac{d\gamma_n}{dt} = v_{\gamma_n}^*, \tag{8}$$

where  $s_{\gamma_n}$  denotes the location of  $\gamma_n$  in the complex  $s$ -plane. Here

$$v_{\gamma_n}^* = -\frac{i\gamma_n \zeta''(s_{\gamma_n})}{4\pi \zeta'(s_{\gamma_n})} + F_{\gamma_n}(s_{\gamma_n}), \tag{9}$$

where primes denote differentiations with  $s$ , and  $F_{\gamma_n}(s_{\gamma_n})$  is given by Eq. (15) with  $k=n$  (see below).

The remaining  $n-1$  vortices composing the trailing edge wake, which have been released from the airfoil edge at earlier times (when  $d\gamma_k/dt, k=1, \dots, n-1$ , changed sign), are treated as “free” vortices: their circulations  $\gamma_k$  are assumed constant and their locations are tracked similar to the incident vortex  $\Gamma$  (see Section 2.3). The total potential induced by the wake is given by the sum

$$w_\gamma(\zeta) = \sum_{k=1}^n \left( -\frac{i\gamma_k}{2\pi} \ln(\zeta - \zeta_{\gamma_k}) + \frac{i\gamma_k}{2\pi} \ln\left(\zeta - \frac{1}{\zeta_{\gamma_k}^*}\right) \right), \tag{10}$$

which includes the potential of  $n$  image vortices of circulations  $-\gamma_k$  placed at the inverse points  $\zeta = 1/\zeta_{\gamma_k}^*$ . The Kutta condition, imposing finite velocity at the airfoil trailing edge, can now be applied. Making use of (2), (4), (5) and (10), and requiring that the diverging part of the flow velocity at the trailing edge vanishes, yields the equation

$$\gamma_n(t) = \frac{2 \operatorname{Re}\{\zeta_{\gamma_n}\} - |\zeta_{\gamma_n}|^2 - 1}{|\zeta_{\gamma_n}|^2 - 1} \left( \frac{2\Gamma(1 - \operatorname{Re}\{\zeta_\Gamma\})}{2 \operatorname{Re}\{\zeta_\Gamma\} - |\zeta_\Gamma|^2 - 1} + 2\pi a \frac{d\xi}{dt} + \sum_{k=1}^{n-1} \frac{\gamma_k(1 - |\zeta_{\gamma_k}|^2)}{2 \operatorname{Re}\{\zeta_{\gamma_k}\} - |\zeta_{\gamma_k}|^2 - 1} \right), \tag{11}$$

which determines the instantaneous circulation of the evolving vortex  $\gamma_n(t)$ . Eqs. (8) and (11) specify the properties of the vortex  $\gamma_n$ .

### 2.3. Formulation of the dynamical problem

Summarizing the above discussion, the dynamical problem consists of  $n+2$  equations for  $n+2$  unknowns, namely the time-dependent locations of the incident vortex  $\Gamma$  and  $n$  trailing edge vortices  $\gamma_k$  ( $k=1, \dots, n$ ), together with the time-varying circulation of the vortex  $\gamma_n$ . Two of the equations have been formulated in (8) (Brown and Michael equation) and (11) (Kutta condition), and the other  $n$  equations are the equations of motion for the  $n$  “free” vortices. We formulate these equations in the  $s$ -plane. Once solved, the results are mapped into the physical  $z$ -plane by taking  $z = s + i\xi$ .

The equation of motion for the incident vortex is obtained by taking the  $s$ -derivative of the flow complex potential in (2), evaluating the result at the vortex location  $s_\Gamma$ , and removing the singular contribution of the vortex self-potential. This procedure yields [27]

$$\frac{ds_\Gamma^*}{dt} = -\frac{i\Gamma \zeta''(s_\Gamma)}{4\pi \zeta'(s_\Gamma)} + F_\Gamma(s_\Gamma), \tag{12}$$

where

$$F_\Gamma(s_\Gamma) = \frac{i\Gamma}{2\pi} \frac{\zeta'_\Gamma}{\zeta_\Gamma^2 - |\zeta_\Gamma|^2} + i \frac{d\xi}{dt} \frac{\zeta'_\Gamma}{\zeta_\Gamma^2} - \frac{i\zeta'_\Gamma}{2\pi} \sum_{k=1}^n \gamma_k \left( \frac{1}{\zeta_\Gamma - \zeta_{\gamma_k}} - \frac{1}{\zeta_\Gamma - 1/\zeta_{\gamma_k}^*} \right) + 1. \tag{13}$$

A similar procedure follows to formulate the equations of motion for the  $n-1$  “free” trailing edge vortices, which take the form

$$\frac{ds_{\gamma_k}^*}{dt} = -\frac{i\Gamma \zeta''(s_{\gamma_k})}{4\pi \zeta'(s_{\gamma_k})} + F_{\gamma_k}(s_{\gamma_k}), \tag{14}$$

with

$$F_{\gamma_k}(s_{\gamma_k}) = -\frac{i\Gamma}{2\pi} \frac{\zeta'_\Gamma}{\zeta_{\gamma_k} - \zeta_\Gamma} \left( \frac{1}{\zeta_{\gamma_k} - \zeta_\Gamma} - \frac{1}{\zeta_{\gamma_k} - 1/\zeta_\Gamma^*} + \frac{1}{\zeta_{\gamma_k}} \right) + \frac{i\gamma_k}{2\pi} \frac{\zeta'_{\gamma_k}}{\zeta_{\gamma_k} - 1/\zeta_{\gamma_k}^*} + i \frac{d\xi}{dt} \frac{\zeta'_{\gamma_k}}{\zeta_{\gamma_k}^2} - \frac{i\zeta'_{\gamma_k}}{2\pi} \sum_{m=1, m \neq k}^n \gamma_m \left( \frac{1}{\zeta_{\gamma_k} - \zeta_{\gamma_m}} - \frac{1}{\zeta_{\gamma_k} - 1/\zeta_{\gamma_m}^*} \right) + 1, \tag{15}$$

and  $k=1, \dots, n-1$ .

The nonlinear system of Eqs. (8), (11), (12) and (14) formulates the dynamical problem to be solved in conjunction with an initial condition for the vortex location at time  $t=0$ . At  $t < 0$ , the airfoil has no trailing edge wake (i.e.,  $n=0$ ), and release of the first trailing edge vortex is initiated at  $t=0$ . The system of equations was integrated numerically using a fourth-order Runge–Kutta algorithm. The typical time step used for integration was  $\pi/250\omega$  (i.e., 500 time steps during each heaving period of the airfoil), which proved sufficient for convergence (with errors  $\lesssim 0.1\%$ ). Notably, the running time required for a single computation (that is, calculation of system evolution for a specific set of parameters from an initial state, when the

vortex is located far upstream of the airfoil, to a time after it has passed past the plate trailing edge) was very short, being only few seconds on a standard desktop machine.

### 3. Acoustic radiation

In the present small-amplitude, low-Mach high-Reynolds number setup, the far-field acoustic pressure is governed by the Powell–Howe acoustic analogy [2,27]

$$\left(\frac{1}{c_0^2} \frac{\partial^2}{\partial t^2} - \nabla^2\right) p = \rho_0 \frac{dv_n}{dt} \delta(x_2) + \rho_0 \nabla \cdot (\boldsymbol{\Omega} \times \mathbf{V}), \quad (16)$$

where  $c_0$  is the speed of sound,  $\rho_0$  is the mean fluid density,  $\delta$  is the Dirac delta function, and  $\mathbf{V}$  is the fluid velocity. Also appearing in (16) is  $\boldsymbol{\Omega}$ , the vector of fluid vorticity, given by the sum of

$$\boldsymbol{\Omega}_I = \hat{\mathbf{x}}_3 \Gamma \delta(\mathbf{x} - \mathbf{x}_I(t)) \quad \text{and} \quad \boldsymbol{\Omega}_\gamma = \sum_{k=1}^n \boldsymbol{\Omega}_{\gamma_k} = \hat{\mathbf{x}}_3 \sum_{k=1}^n \gamma_k \delta(\mathbf{x} - \mathbf{x}_{\gamma_k}(t)), \quad (17)$$

which mark the incident and trailing edge vorticities, respectively. In accordance with Eq. (17) and the linearity of Eq. (16), the acoustic pressure can be written as a sum of “airfoil motion”, “incident vortex”, and “wake” contributions,

$$p(\mathbf{x}, t) = p_{v_n}(\mathbf{x}, t) + p_I(\mathbf{x}, t) + p_\gamma(\mathbf{x}, t), \quad (18)$$

where

$$p_{v_n}(\mathbf{x}, t) = \rho_0 \frac{\partial}{\partial t} \int_0^\infty v_n(\tau) f_{S_a} G(\mathbf{x}, \mathbf{y}, t - \tau) dS(\mathbf{y}) d\tau, \quad (19)$$

$$p_I(\mathbf{x}, t) = -\rho_0 \int_0^\infty \int_{\mathcal{V}_I} (\boldsymbol{\Omega}_I \times \mathbf{V}_I) \cdot \frac{\partial G}{\partial \mathbf{y}}(\mathbf{x}, \mathbf{y}, t - \tau) d\mathbf{y} d\tau, \quad (20)$$

and

$$p_\gamma(\mathbf{x}, t) = -\rho_0 \sum_{k=1}^n \int_0^\infty \int_{\mathcal{V}_{\gamma_k}} (\boldsymbol{\Omega}_{\gamma_k} \times \mathbf{V}_{\gamma_k}) \cdot \frac{\partial G}{\partial \mathbf{y}}(\mathbf{x}, \mathbf{y}, t - \tau) d\mathbf{y} d\tau. \quad (21)$$

In (19)–(20),  $S_a$  is the airfoil surface,  $\mathcal{V}_I$  and  $\mathcal{V}_{\gamma_k}$  denote the fluid regions occupied by the trailing edge and incident vortices, respectively,  $G(\mathbf{x}, \mathbf{y}, t - \tau)$  is the acoustic Green's function having a vanishing normal derivative on the undisturbed plate, and  $\mathbf{V}_I$  and  $\mathbf{V}_{\gamma_k}$  are the incident and trailing edge vortex velocities, respectively.

To proceed with the evaluation of the acoustic pressure, we consider a case where the airfoil is acoustically compact. Thus, we assume that  $a/\lambda \ll 1$ , where  $\lambda = 2\pi/k$  is the dimensional acoustic wavelength, and  $k = \omega/c_0$  is the dimensional acoustic wavenumber. The condition for airfoil compactness is then given by  $a/\lambda = M(\omega a/2\pi U) \ll 1$ , where  $M = U/c_0$  is the mean stream Mach number. This restriction is in accordance with the low Mach assumption set in (16). The compact approximation of Green's function [27]

$$G(\mathbf{x}, \mathbf{y}, t - \tau) = \frac{1}{4\pi|\mathbf{X} - \mathbf{Y}|} \delta\left(t - \tau - \frac{|\mathbf{X} - \mathbf{Y}|}{c_0}\right) \quad (22)$$

is applied to evaluate the acoustic radiation, where  $\mathbf{X}(\mathbf{x})$  and  $\mathbf{Y}(\mathbf{y})$  are the Kirchhoff vectors for the plate. To make use of (22) in the present two-dimensional configuration, the above Green's function is integrated over  $-\infty < y_3 < \infty$ . Taking the far-field ( $|\mathbf{X}| \sim |\mathbf{x}| \rightarrow \infty$ ) limit, the leading-order Green's function contributing to the dipole acoustic field is

$$G(\mathbf{x}, \mathbf{y}, t - \tau) \approx \frac{\mathbf{x} \cdot \mathbf{Y}}{2\pi\sqrt{2c_0}|\mathbf{x}|^{3/2}} \frac{\partial}{\partial t} \left\{ \frac{H([t] - \tau)}{\sqrt{[t] - \tau}} \right\}, \quad |\mathbf{x}| \rightarrow \infty, \quad (23)$$

where  $[t] = t - |\mathbf{x}|/c_0$  is the *acoustic retarded time*. We approximate  $\mathbf{Y}(\mathbf{y})$  by the two-dimensional Kirchhoff vector for a strip,

$$\mathbf{Y}(\mathbf{y}) = \left( y_1, \operatorname{Re} \left\{ -i\sqrt{(y_1 + iy_2)^2 - a^2} \right\} \right). \quad (24)$$

To evaluate  $p_{v_n}(\mathbf{x}, t)$ , substitute (23) into (19) and specify the path of integration. The space integral can be calculated explicitly to yield

$$p_{v_n}(\mathbf{x}, t) \approx \frac{\rho_0 a^2 \cos \theta}{2\sqrt{2c_0}|\mathbf{x}|} \frac{\partial^2}{\partial t^2} \int_0^{[t]} \frac{d\xi/d\tau}{\sqrt{[t] - \tau}} d\tau, \quad (25)$$

where  $\cos \theta = x_2/|\mathbf{x}|$ , and  $0 \leq \theta \leq \pi$  indicates the observer direction. Substituting (1) into (25), the time integral can be evaluated for long times, yielding

$$p_{v_n}(\mathbf{x}, [t] \rightarrow \infty) \approx \frac{\sqrt{2\pi}\rho_0 a^3 \cos \theta}{4\sqrt{c_0}|\mathbf{x}|} \bar{\varepsilon} \omega^{5/2} \sin\left(\omega[t] - \frac{\pi}{4}\right). \quad (26)$$

In practice, this “long time” approximation becomes valid already after few heaving periods of the airfoil.

Unlike the analytical evaluation for  $p_{v_n}$ , the calculation of incident vortex and wake contributions to acoustic pressure must be carried out numerically, based on the scheme described in Section 2. To evaluate  $p_r$ , substitute (23) together with (17) into (20) to obtain

$$p_r(\mathbf{x}, t) \approx \frac{\rho_0 \Gamma \sin \theta}{2\pi \sqrt{2c_0 |\mathbf{x}|}} \frac{\partial}{\partial t} \int_0^{[t]} \frac{V_r^{(2)}(\tau) d\tau}{\sqrt{[t]-\tau}} - \frac{\rho_0 \Gamma \cos \theta}{2\pi \sqrt{2c_0 |\mathbf{x}|}} \frac{\partial}{\partial t} \int_0^{[t]} \left( V_r^{(1)}(\tau) \frac{\partial Y_2}{\partial y_2} - V_r^{(2)}(\tau) \frac{\partial Y_2}{\partial y_1} \right)_{\mathbf{x}_r(\tau) \sqrt{[t]-\tau}} \frac{d\tau}{\sqrt{[t]-\tau}}, \tag{27}$$

where  $V_r^{(j)}$  denotes the velocity component of the incident vortex in the  $x_j$ -direction. Similarly,  $p_\gamma$  is evaluated by substituting (23) and (17) into (21), to yield

$$p_\gamma(\mathbf{x}, t) \approx \sum_{k=1}^n \left( \frac{\rho_0 \gamma_k \sin \theta}{2\pi \sqrt{2c_0 |\mathbf{x}|}} \frac{\partial}{\partial t} \int_0^{[t]} \frac{V_{\gamma_k}^{(2)}(\tau) d\tau}{\sqrt{[t]-\tau}} - \frac{\rho_0 \gamma_k \cos \theta}{2\pi \sqrt{2c_0 |\mathbf{x}|}} \frac{\partial}{\partial t} \int_0^{[t]} \left( V_{\gamma_k}^{(1)}(\tau) \frac{\partial Y_2}{\partial y_2} - V_{\gamma_k}^{(2)}(\tau) \frac{\partial Y_2}{\partial y_1} \right)_{\mathbf{x}_{\gamma_k}(\tau) \sqrt{[t]-\tau}} \frac{d\tau}{\sqrt{[t]-\tau}} \right), \tag{28}$$

where  $V_{\gamma_k}^{(j)}$  denotes the velocity component of the vortex  $\gamma_k$  in the  $x_j$ -direction.

The integral terms appearing in (27) and (28) are directly related to the two components of unsteady force exerted on the fluid (per unit span) by the airfoil: the  $\sin \theta$  terms are directed along the airfoil chord and represent the influence of “suction” forces at the leading and trailing edges; the  $\cos \theta$  terms represent the unsteady lift experienced by the airfoil during its interaction with the incident vortex and wake. The suction-type dipole appearing in (27) and (28) is in marked difference from expression (25) for  $p_{v_n}$ , which contains only a lift-dipole term. This difference is attributed to the nonlinear vortex-airfoil interactions, leading to velocity components of the incident and trailing edge vortices in the normal  $x_2$ -direction. Consequently, dipole-type sound is radiated in the  $x_1$ -direction, reflecting both incident vortex motion at times when the vortex passes close to the airfoil (in which  $V_r^{(2)} \neq 0$ ) and heaving airfoil motion which causes the trailing edge vortices to move in the  $x_2$ -direction (having  $V_{\gamma_k}^{(2)} \neq 0$ ).

4. Results

To non-dimensionalize the problem, the length, velocity and time are scaled by  $a$ ,  $U$  and  $a/U$ , respectively. Marking non-dimensional quantities by overbars, the non-dimensional problem is governed by

$$\bar{\varepsilon}, \quad \bar{\omega} = \frac{\omega a}{U}, \quad \bar{\Gamma} = \frac{\Gamma}{2\pi a U} \quad \text{and} \quad \bar{\mathbf{x}}_r(0) = \frac{\mathbf{x}_r(0)}{a}, \tag{29}$$

denoting the normalized amplitude and frequency of airfoil motion, and the incident vortex circulation and initial location, respectively. Adopting this scaling, the non-dimensional form of the acoustic pressure (18) is

$$\frac{p(\mathbf{x}, t)}{\rho_0 U^2} = \sqrt{\frac{M}{8|\bar{\mathbf{x}}|}} \Pi_{\text{tot}}([\bar{t}]) = \sqrt{\frac{M}{8|\bar{\mathbf{x}}|}} (\Pi_{v_n}([\bar{t}]) + \Pi_r([\bar{t}]) + \Pi_\gamma([\bar{t}]}), \tag{30}$$

where

$$\Pi_{v_n}([\bar{t}]) \approx \cos \theta \frac{\partial^2}{\partial \bar{t}^2} \int_0^{[\bar{t}]} \frac{d\bar{\xi}/d\tau}{\sqrt{[\bar{t}]-\tau}} d\tau, \tag{31}$$

$$\Pi_r([\bar{t}]) \approx 2\bar{\Gamma} \left( \sin \theta \frac{\partial}{\partial \bar{t}} \int_0^{[\bar{t}]} \frac{\bar{V}_r^{(2)} d\tau}{\sqrt{[\bar{t}]-\tau}} - \cos \theta \frac{\partial}{\partial \bar{t}} \int_0^{[\bar{t}]} \frac{(\bar{V}_r^{(1)} + i\bar{V}_r^{(2)}) \bar{z}_r d\tau}{\sqrt{(\bar{z}_r^2 - 1)([\bar{t}]-\tau)}} \right), \tag{32}$$

and

$$\Pi_\gamma([\bar{t}]) \approx \sum_{k=1}^n 2\bar{\gamma}_k \left( \sin \theta \frac{\partial}{\partial \bar{t}} \int_0^{[\bar{t}]} \frac{\bar{V}_{\gamma_k}^{(2)} d\tau}{\sqrt{[\bar{t}]-\tau}} - \cos \theta \frac{\partial}{\partial \bar{t}} \int_0^{[\bar{t}]} \frac{(\bar{V}_{\gamma_k}^{(1)} + i\bar{V}_{\gamma_k}^{(2)}) \bar{z}_{\gamma_k} d\tau}{\sqrt{(\bar{z}_{\gamma_k}^2 - 1)([\bar{t}]-\tau)}} \right). \tag{33}$$

In (33),  $\bar{\gamma}_k = \gamma_k/(2\pi a U)$ . In the limit  $[\bar{t}] \rightarrow \infty$ , the expression for  $\Pi_{v_n}$  in (31) becomes

$$\Pi_{v_n}([\bar{t}] \rightarrow \infty) \approx \sqrt{\pi \bar{\varepsilon}} \bar{\omega}^{5/2} \cos \theta \sin \left( \bar{\omega} [\bar{t}] - \frac{\pi}{4} \right), \tag{34}$$

which is the non-dimensional counterpart of Eq. (26).

The results for the acoustic pressure will be presented in terms of the acoustic “kernels”  $\Pi_{\text{tot}}$ ,  $\Pi_{v_n}$ ,  $\Pi_r$  and  $\Pi_\gamma$ . The non-dimensional acoustic pressure is governed, in addition to the parameters specified in (29), by the observer direction  $\theta = \cos^{-1}(x_2/|\mathbf{x}|)$ . To illustrate our findings we focus on a case of an incident vortex initially located at  $\mathbf{x}_r(0)/a = (-20, 0.2)$ , sufficiently far upstream of the airfoil, where it essentially convects with the mean flow. In addition, we fix  $\Gamma/(2\pi a U) = 0.2$  and  $\bar{\varepsilon} = 0.01$  (or otherwise consider the case of a stationary airfoil,  $\bar{\varepsilon} = 0$ ), in accordance with our preliminary small-amplitude-motion assumption. The remaining free parameter is therefore the normalized heaving frequency  $\omega a/U$ . We start by analysing the dynamical and acoustic problems for a stationary airfoil, and then examine the case of a heaving airfoil, to illustrate the added effects of boundary animation.

#### 4.1. The case $\bar{\epsilon} = 0$

When  $\bar{\epsilon} = 0$ , release of trailing edge vorticity results only from airfoil interaction with the incident vortex. This interaction is expected to be most intense when the vortex passes close to the structure, and in particular when it passes in the proximity of airfoil end points. To examine this behaviour, Figs. 2 and 3 present the flow-field and acoustic radiation of a stationary airfoil.

The incident vortex trajectory is shown by the solid line in Fig. 2a. As the vortex is placed in the flow at  $t=0$ , it induces fluid loading on the airfoil, resulting in generation of trailing edge vorticity. Satisfaction of the Kutta condition (11) and Brown and Michael equation (8) determines the evolution of the trailing edge vortex  $\gamma_1$ . The trajectory and circulation of  $\gamma_1$  are presented by the dash-dotted lines in Fig. 2b and c, respectively. When the incident vortex approaches the airfoil in the mean-flow direction, it slightly shifts in the upward  $x_2$ -direction owing to the vortex force  $\Omega \times \mathbf{U}$  induced by the image vorticity at  $\zeta(z) = 1/\zeta^*(z_r)$  (see (4)). At this stage, the trailing edge vortex moves away from the airfoil while its circulation increases monotonically. When the incident vortex reaches  $\mathbf{x}_r/a \approx (-4.9, 0.21)$ , the trailing edge vortex trajectory changes direction, and starts moving back towards the airfoil. This is accompanied by a decrease in the value of  $d\gamma_1/dt$ . Shortly after the incident vortex has passed above the airfoil leading edge (at  $Ut/a \approx 19.4$ , marked by crosses),  $d\gamma_1/dt$  changes sign: at this time instant, the interaction of the incident vortex with the airfoil trailing edge (which at earlier times was weaker than its interaction with the leading edge) becomes dominant, and the  $\gamma_1$ -vortex is detached from the trailing edge. Keeping its final circulation  $\gamma_1 \approx 0.59\Gamma$  constant at later times (see the dash-dotted line in Fig. 2c), it then convects as a “free” vortex, while shedding of  $\gamma_2$  (having negative circulation) is initiated. Time evolution of  $\gamma_2$ , characterized by a sharp change in its circulation (see the dashed line in Fig. 2c), continues until slightly after the incident vortex has passed above the airfoil trailing edge. At time  $Ut/a \approx 21.3$ , marked by triangles in the figure,  $d\gamma_2/dt$  changes sign, followed by detachment of  $\gamma_2$  from the trailing edge and release of  $\gamma_3 > 0$ . Our calculations indicate that no additional vortices need to form at the trailing edge at later times, since  $\gamma_3$  is monotonically increasing for  $Ut/a \gtrsim 21.3$ . Notably, while the trajectories of  $\gamma_1$  and  $\gamma_3$  remain in the vicinity of the  $x_1$ -axis (note the difference in scales between the  $x_1$ - and  $x_2$ -axes in Fig. 2b), the trajectory of  $\gamma_2$  (having circulation opposite in sign to  $\Gamma$ ) follows the path of the incident vortex (see the location of the two vortices at  $Ut/a = 25$ , marked by the squares in Fig. 2a). As will be demonstrated in Fig. 3, this results in suppression of the acoustic field radiated by the incident vortex.

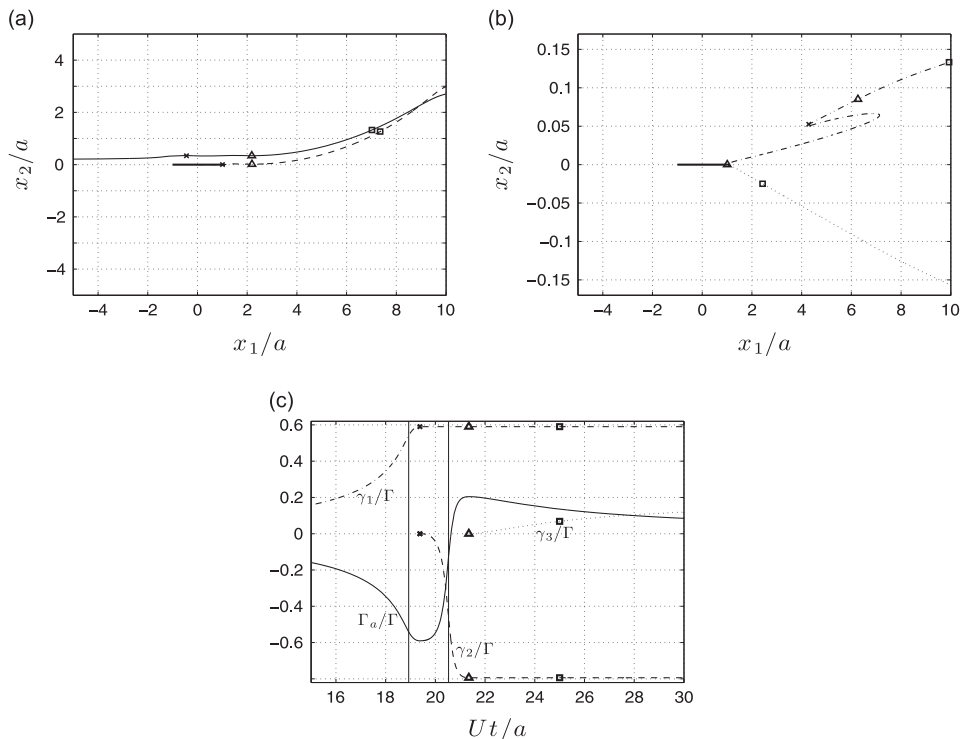


**Fig. 2.** Flow-field induced by an incident vortex passing past a stationary plate: (a) trajectories of incident vortex (solid) and trailing edge vortex  $\gamma_2$  (dashed); (b) trajectories of trailing edge vortices  $\gamma_1$  (dash-dotted) and  $\gamma_3$  (dotted); (c) time variations of airfoil circulation (solid line) and trailing edge vortex circulations (dashed, dash-dotted and dotted curves). The bold solid lines in Fig. 2a and b indicate the airfoil location. The crosses, triangles and squares denote the vortex locations (Fig. 2a and b) and circulations (Fig. 2c) at times  $Ut/a \approx 19.4, 21.3$  and 25, respectively. The vertical solid lines in Fig. 2c confine the time interval during which the incident vortex passes above the airfoil.

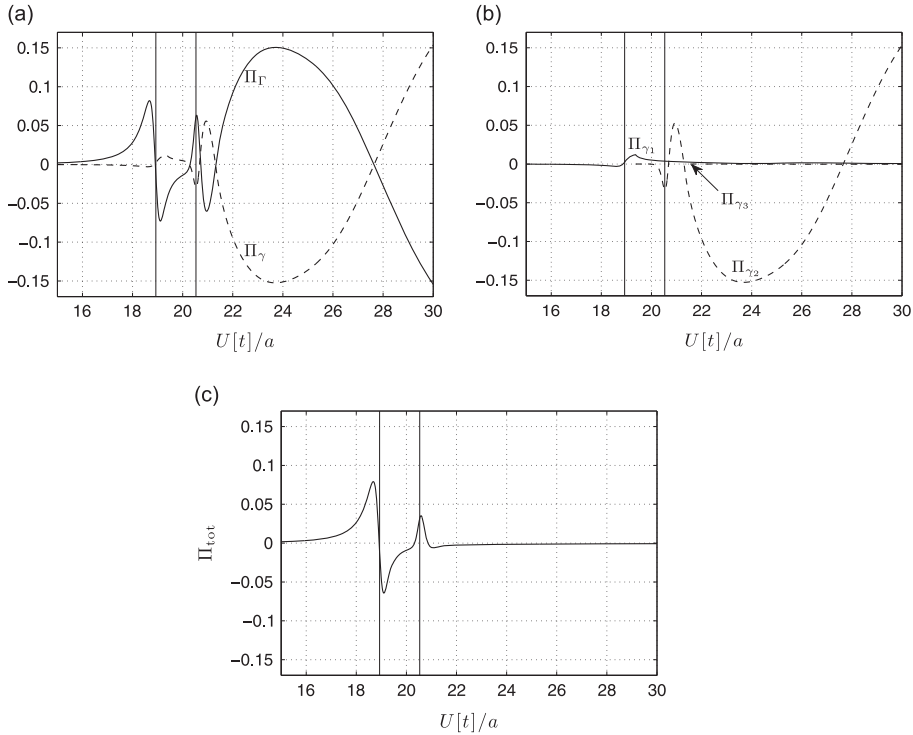


**Fig. 3.** Acoustic signature of a stationary airfoil along  $\theta = \pi/2$  (suction dipole): (a) separate incident vortex ( $\Pi_\Gamma$ , solid line) and wake ( $\Pi_\gamma$ , dashed line) contributions; (b) decomposition of  $\Pi_\gamma$  into separate contributions from trailing edge vortices  $\Pi_{\gamma_{1,2,3}}$ ; (c) total acoustic signature. The vertical solid lines in each part confine the time interval during which the incident vortex passes above the airfoil.

In addition to the time-variations of trailing-edge vortex circulations, the solid line in Fig. 2c presents the airfoil circulation  $\Gamma_a(t)$ , normalized by  $\Gamma$ . In accordance with Kelvin's theorem,

$$\Gamma_a(t) = - \sum_{k=1}^n \gamma_k(t), \quad (35)$$

which satisfies the condition that  $\Gamma_a(0) = 0$ . The non-monotonic changes in  $\Gamma_a$  reflect the detachments of trailing edge vortices: at  $0 \leq Ut/a \leq 19.4$  the circulation decreases from  $\Gamma_a(0) = 0$  to  $\Gamma_a \approx -0.59\Gamma$ . It then increases to  $\Gamma_a \approx 0.2\Gamma$  as  $\gamma_2$  is released, and decreases again for  $Ut/a \geq 21.3$ . At late times  $\Gamma_a \rightarrow 0$ , as the loading induced by the incident vortex on the airfoil vanishes. The time-variation for  $\Gamma_a$  calculated here, a manifestation of the unsteady lift force experienced by the airfoil, is in marked difference from a previous analysis of the problem [23], where the effect of trailing-edge wake has been neglected at the outset, and the airfoil circulation was assumed zero at all times.

The acoustic radiation of a stationary-airfoil system is presented in Fig. 3, where we focus on the suction dipole oriented along the  $x_1$ -axis ( $\theta = \pi/2$ ). In general,  $\Pi_{v_n} = 0$  for a stationary airfoil, and the total signal  $\Pi_{tot}$ , shown in Fig. 3c, is the sum of incident vortex ( $\Pi_\Gamma$ ) and wake ( $\Pi_\gamma = \sum_{k=1}^n \Pi_{\gamma_k}$ ) radiations. The separate contributions of  $\Pi_\Gamma$  and  $\Pi_\gamma$  are shown by the solid and dashed curves in Fig. 3a, respectively, and the decomposition of  $\Pi_\gamma$  into the separate acoustic radiations of trailing edge vortices  $\Pi_{\gamma_{1,2,3}}$  is presented in Fig. 3b.

Starting with the incident vortex radiation (see solid line in Fig. 3a), we find that at early times the vortex convects with the constant mean velocity  $\mathbf{U} = U\hat{\mathbf{x}}_1$  and does not generate sound. When the vortex approaches the airfoil leading edge, its trajectory is shifted upwards (see Fig. 2a), and considerable pressure fluctuations are generated during its interactions with the airfoil end points (at times marked by the two vertical lines). Once the vortex has passed over the plate, it continues radiating sound along its trajectory, mainly due to its interaction with the trailing edge vortex  $\gamma_2$  (see the trajectories in Fig. 2a). Considering the decomposition of wake sound  $\Pi_\gamma$  into  $\Pi_{\gamma_{1,2,3}}$  presented in Fig. 3b, we observe that its dominant component is  $\Pi_{\gamma_2}$  which, clearly, cancels out  $\Pi_\Gamma$  at late times (after the passage of incident vortex above the airfoil). Consequently, the total pressure signal presented in Fig. 3c reflects only the vortex interactions with the airfoil leading and trailing edges. The interaction with the trailing edge generates a relatively weaker pressure fluctuation owing to partial suppression caused by  $\Pi_\gamma$  (cf. the sum of the solid and dashed lines in Fig. 3a in the vicinity of the right vertical line). This suppression is only partial since, at this stage, the vortex  $\gamma_2$  is still evolving (not yet detached from the trailing edge), and its strength is relatively weak.

Howe [32] applied the emended Brown and Michael equation to study the acoustic radiation of a line vortex convected past the edge of a stationary semi-infinite plate with no mean flow. No leading edge interaction existed in this semi-infinite

configuration, and it was shown that trailing edge wake could be represented by shedding of only one vortex. More recently, Guo [33] considered the sound radiated from a line vortex passing past a stationary Joukowski airfoil, through the application of the emended Brown and Michael equation and a two-dimensional formulation of the Ffowcs Williams–Hawkings analogy. In support of the present analysis, the results in Refs. [32,33] demonstrate the suppressing effect of trailing edge vorticity on the total acoustic radiation. In particular, in the finite-airfoil configuration considered by Guo, it was found that trailing edge wake can be described by shedding of three vortices, which circulations and trajectories are qualitatively similar to those presented in Fig. 2 (cf. Figs. 3–5 in Ref. [33]). This agreement lends support of the following application of our scheme to evaluate the acoustic far field of a heaving airfoil.

#### 4.2. The case $\bar{e} \neq 0$

Airfoil heaving has both direct and indirect effects on the system vibroacoustic behaviour: directly, airfoil vibration radiates sound, given by  $\Pi_{v_n}$  in Eq. (31); indirectly, heaving motion influences the incident vortex trajectory and results in release of additional trailing edge vorticity which, in turn, affects both near-field flow and far-field acoustic signature. Our numerical calculations indicate that the impact of airfoil heaving is minor at low frequencies  $\omega a/U \ll 1$ , and we therefore focus on cases where  $\omega a/U \gtrsim O(1)$ .

Fig. 4 presents the flow-field induced by an incident vortex passing past a heaving airfoil with  $\omega a/U = 1$ . Fig. 4a–c shows the locations of incident and trailing edge vortices at different time instants. For easy reference, trailing edge vortices with positive and negative circulations are marked by crosses and triangles, respectively. At each time snapshot, the airfoil location is marked by a bold horizontal line, and the incident vortex trajectory is shown by a thin curve. The trajectory of the trailing edge vortex  $\gamma_6$ , shed when the incident vortex passes above the airfoil trailing edge, is depicted by the dashed lines. Fig. 4d complements the flow-field description by presenting time variation of scaled airfoil circulation  $\Gamma_a/\Gamma$ . To illustrate the effect of heaving frequency, total circulations are also presented for a stationary wing (dashed line; identical with the solid curve appearing in Fig. 2c) and a heaving airfoil with  $\omega a/U = 1.5$  (dotted line).

Airfoil heaving results in continuous release of trailing edge vorticity. According to the present calculation, two vortices are detached from airfoil trailing edge during each heaving period. The detachments account for changes in sign of  $d^2\xi/dt^2$  during a period, causing changes in sign of  $d\gamma_n/dt$  of the released vortex (see the time derivative of Eq. (11) after removing

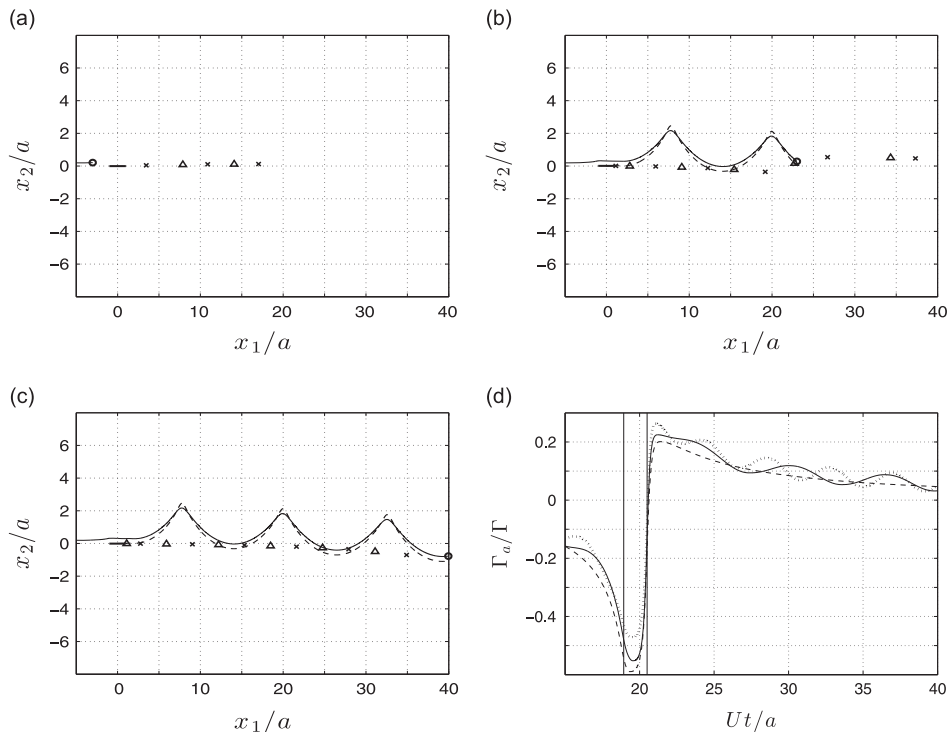


**Fig. 4.** Flow-field induced by an incident vortex passing past a heaving airfoil with  $\omega a/U = 1$ : (a–c) locations of incident vortex (circle) and trailing edge vortices (crosses and triangles) at times  $Ut/a \approx 17$  (Fig. 4a),  $Ut/a \approx 43$  (Fig. 4b), and  $Ut/a \approx 59$  (Fig. 4c). The crosses and triangles denote vortices with positive and negative circulations, respectively. The solid and dashed curves show trajectories of incident vortex and vortex  $\gamma_6$  (released when the incident vortex passes above the airfoil trailing edge), respectively. The bold solid line in each figure indicates the instantaneous airfoil location (which appears unchanged owing to the large scale of the  $x_2$ -axis presented). (d) Time variations of scaled airfoil circulation for  $\omega a/U = 1$  (solid line),  $\omega a/U = 1.5$  (dotted line), and a stationary airfoil (dashed line). Vertical solid lines confine the time interval during which the incident vortex passes above the airfoil for  $\omega a/U = 1$ .

the incident vortex and the other (relatively minor) trailing edge vortex contributions). Accordingly, at the time  $Ut/a \approx 17$  presented in Fig. 4a, approximately  $17/2\pi \approx 2.7$  heaving periods have elapsed, and five vortices of alternating signs have been released. These vortices form the beginning of a “vortex street”, characterizing the wake behind oscillating bodies. When the incident line vortex approaches the airfoil, additional fluid loading is induced on the airfoil, which affects the shedding of trailing edge vorticity. The effect of incident vortex on trailing edge wake is similar in essence to that described in Fig. 2: as the vortex passes above the airfoil, its interaction with the trailing edge becomes dominant; the release of a new trailing edge vortex (in this case,  $\gamma_6$ ) is initiated and continues until shortly after the incident vortex has passed above the airfoil trailing edge;  $\gamma_6$  is then detached from the trailing edge and forms a “vortex-pair” motion with the incident vortex (cf. the solid and dashed lines in Fig. 4a and b); this motion effectively cancels out the incident vortex sound at late times, as will be demonstrated in Fig. 5. After the vortex pair has moved away from the airfoil, release of trailing edge vorticity continues in accordance with the airfoil heaving motion. The time variation of scaled airfoil circulation  $\Gamma_a/\Gamma$ , shown by the solid line in Fig. 4d, reflects both strong vortex-airfoil interaction at the time when the vortex passes above the airfoil, and periodic release of vorticity at the heaving frequency (cf. the solid line in Fig. 2c). Evidently, the effect of periodic release of trailing edge vortices, reflecting heaving motion, is missing in the non-heaving case (dashed line), and becomes more pronounced with increasing  $\omega$ , as in the  $\omega a/U = 1.5$  setup (dotted line). At late times (when the effect of incident vortex becomes negligible),  $\Gamma_a$  varies periodically in each of the heaving-airfoil configurations, with its mean value  $\Gamma_a \rightarrow 0$ .

Fig. 5 presents the far-field acoustic radiation of an incident vortex interacting with a heaving airfoil at  $\omega a/U = 1$  (same as in Fig. 4). Fig. 5a and b presents separate contributions of incident vortex (solid lines), trailing edge wake (dashed lines) and airfoil motion (dash-dotted line) radiations to the lift (Fig. 5a) and suction (Fig. 5b) dipoles. Fig. 5c shows decomposition of the trailing edge radiation into contributions from the vortex  $\gamma_6$  (released when the incident vortex passes above the airfoil trailing edge, as found in Fig. 4) and all other trailing edge vortices. Fig. 5d presents the total acoustic signal radiated along the  $x_1$  (dashed line) and  $x_2$  (solid curve) directions.

Starting with Fig. 5a and b, we note, as observed in Section 3, that there is no contribution of airfoil motion sound  $\Pi_{v_n}$  to the suction dipole (see Eq. (31)). Thus, in the present level of approximation, dipole sound is emitted along the mean-flow direction only due to incident vortex and wake radiations. In both Fig. 5a and b,  $\Pi_\Gamma$  and  $\Pi_\gamma$  show similar qualitative behaviour: at early times  $\Pi_\Gamma$  and  $\Pi_\gamma$  are small and the acoustic field is dominated by the direct airfoil sound  $\Pi_{v_n}$  oriented in the  $x_2$ -direction (at the time interval presented, the analytic approximation (34) of  $\Pi_{v_n}$  is identical with the numerical

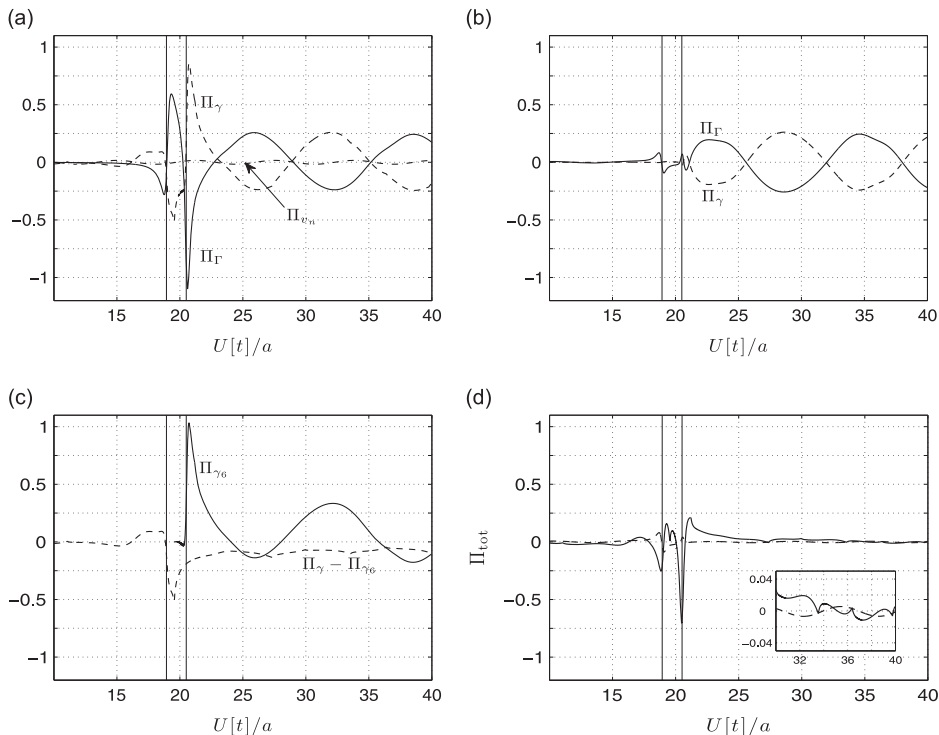


**Fig. 5.** Acoustic signature of an incident vortex passing past a heaving airfoil with  $\omega a/U = 1$ : (a,b) separate incident vortex ( $\Pi_\Gamma$ , solid lines), wake ( $\Pi_\gamma$ , dashed lines) and airfoil-motion ( $\Pi_{v_n}$ , dash-dotted line) contributions to the lift ( $\theta = 0$ , Fig. 5a) and suction ( $\theta = \pi/2$ , Fig. 5b) dipoles; (c) decomposition of  $\Pi_\gamma$  along  $\theta = 0$  into separate contributions from  $\Pi_{\gamma_6}$  (solid line) and all other trailing edge vortices  $\Pi_\gamma - \Pi_{\gamma_6}$  (dashed curve); (d) total acoustic signature along  $\theta = 0$  (solid) and  $\theta = \pi/2$  (dashed). The inset in Fig. 5d shows a close-up on the total acoustic radiation at late times ( $30 \leq U[t]/a \leq 40$ ), and the vertical solid lines in each figure indicate the time interval during which the incident vortex passes above the airfoil.

expression (31)). When the incident vortex approaches the airfoil leading edge, and as it passes above it, large variations in  $\Pi_r$  occur. These are partially cancelled by the release of  $\gamma_6$ , initiated slightly after the incident vortex has passed above the airfoil leading edge (cf. the solid and dashed lines in Fig. 5a and b). Similar to the result in Fig. 3, once the incident vortex has passed the airfoil trailing edge it is “followed” by the vortex  $\gamma_6$ , creating a “silent” vortex pair. As illustrated in Fig. 5c, the acoustic pressure generated by  $\gamma_6$  is considerably larger than radiation from all other trailing edge vortices. At late times, sound radiation is dominated by the airfoil motion in the  $x_2$ -direction. Notably, a closer look into the dashed curve in the inset of Fig. 5d indicates that “indirect” heaving sound is also radiated in the  $x_1$ -direction at late times. This radiation originates from the  $x_2$ -velocity component of trailing edge vortices (see Eq. (33)), induced by the nonlinear interaction between the trailing edge vortices and the airfoil. The total acoustic signature presented in Fig. 5d can therefore be viewed as a combination of “heaving sound” at early and late times, superposed by relatively strong leading and trailing edge interaction fluctuations. Trailing edge vorticity acts to reduce pressure fluctuations generated by the incident vortex, while transmitting sound in both lift and suction directions, which reflects airfoil motion.

To complete the presentation of results, Fig. 6 examines the effect of airfoil heaving frequency  $\omega a/U$  on the total lift (Fig. 6a) and suction (Fig. 6b) dipoles. The solid and dash-dotted lines in each figure mark the acoustic signals for  $\omega a/U = 1$  and  $\omega a/U = 3$ , respectively. The dashed lines present lift and suction dipoles for a stationary airfoil (with the dashed line in Fig. 6b identical with the solid line in Fig. 3c). Fig. 6c presents separate contributions of  $\Pi_{v_n}$  to the lift dipole for both stationary (where  $\Pi_{v_n} \equiv 0$ ) and heaving airfoils. Note the difference in scale between Fig. 6a and b, indicating that the lift dipole is typically much stronger than the suction dipole. As has been demonstrated by Fig. 5, late-time acoustic radiation along the  $x_1$ -direction may originate only from the motion of trailing edge vortices in the  $x_2$ -direction.

Focusing on Fig. 6a and c, we observe that the increase in  $\omega a/U$  magnifies the relative contribution of airfoil heaving sound  $\Pi_{v_n}$  to the lift dipole significantly, while the relative contributions of incident vortex and wake radiations become weaker. The large increase in direct airfoil-motion sound is in accordance with Eq. (34), showing that  $\Pi_{v_n} \sim O(\omega a/U)^{5/2}$ . Nevertheless, vortex sound remains the only source radiating sound along the  $x_1$ -direction, as shown in Fig. 6b. In this direction, the signal is combined of a heaving-frequency component at early and late times, together with vortex-airfoil interaction sound at times when the incident vortex passes in the vicinity of the airfoil. The former effect is inevitably missing in the stationary-airfoil signature shown by the dashed curve (see also the comparison in Fig. 4d between airfoil circulations in heaving and non-heaving setups). With increasing heaving frequencies ( $\omega a/U \gg 1$ ), our results indicate that vortex sound remains significant mainly along the mean-flow direction, while radiation in other directions is dominated by the direct airfoil-motion contribution  $\Pi_{v_n}$ .

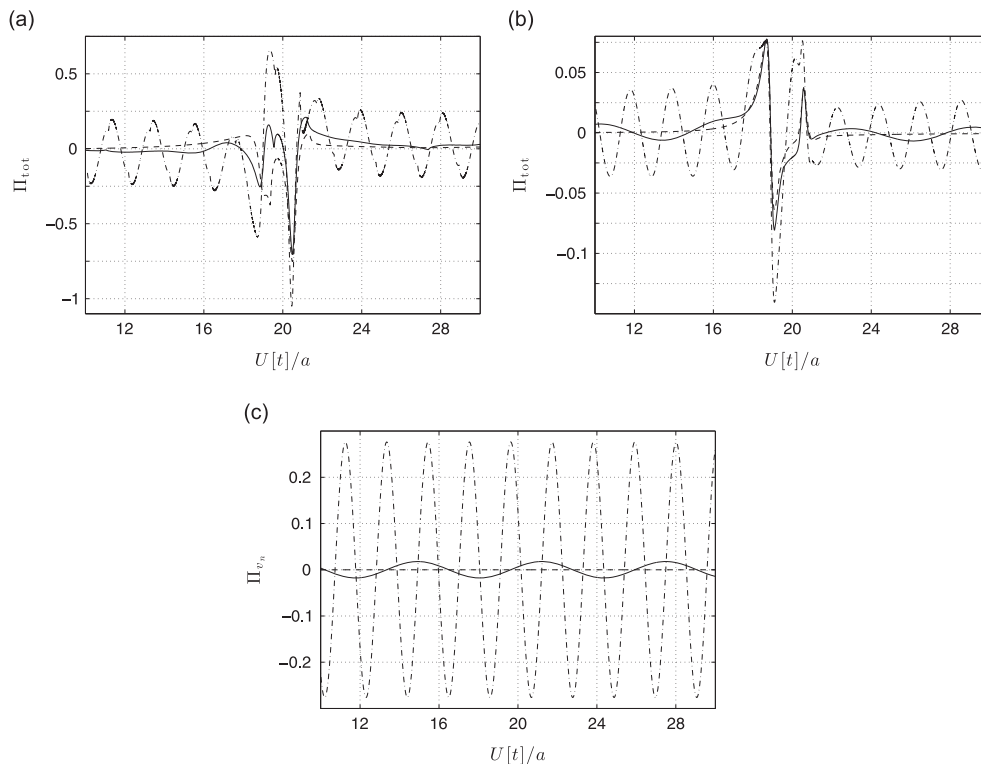


**Fig. 6.** Effect of heaving frequency on the acoustic signature of a heaving airfoil: (a,b) comparison between total lift ( $\theta = 0$ , Fig. 6a) and suction ( $\theta = \pi/2$ , Fig. 6b) dipoles for stationary (dashed line) and heaving ( $\omega a/U = 1$ , solid line;  $\omega a/U = 3$ , dash-dotted line) airfoils. (c) Separate contributions of  $\Pi_{v_n}$  to the lift dipole for stationary (dashed line) and heaving ( $\omega a/U = 1$ , solid line;  $\omega a/U = 3$ , dash-dotted line) airfoils.

## 5. Conclusion

We analysed the effects of flow unsteadiness and periodic boundary animation (small-amplitude heaving) on the vibroacoustic signature of a thin rigid airfoil in low-Mach high-Reynolds number flow. Modeling the incoming flow unsteadiness by an incident line vortex, the dynamical problem for the vortex motion and trailing edge wake evolution was studied using the method of conformal mapping and the Brown and Michael equation. The acoustic problem was then analysed based on Powell–Howe acoustic analogy. The results identify the fluid-airfoil system as a dipole-type source, and show that its behaviour can be divided into two characteristic regimes, based on the scaled heaving frequency  $\omega a/U$ : (i) for  $\omega a/U \ll 1$ , the effect of heaving is minor, and the acoustic response is well approximated by considering the interaction of a line vortex with a stationary airfoil; (ii) for  $\omega a/U \gg 1$ , the impact of heaving is dominant, radiating sound through a direct “airfoil-motion” dipole ( $\propto (\omega a/U)^{5/2}$ ) oriented along the direction of heaving. In this case, vortex sound remains significant only in the vicinity of mean-flow direction. For  $\omega a/U \sim O(1)$ , an intermediate regime takes place, where the influences of both regimes are of comparable strength (see Fig. 5).

The application of the Brown and Michael equation to model the wake dynamics has enabled a detailed study of the effect of nonlinear vortex-airfoil interaction on the system acoustic radiation. It was found that trailing edge vorticity acts to reduce pressure fluctuations generated by the incident vortex interaction with the airfoil. Simultaneously, the motion of trailing edge vortices in the airfoil-motion direction transmits heaving-frequency sound along the mean-flow direction. The “silencing” effect of trailing edge vorticity was found particularly efficient when the incident vortex passes above the airfoil trailing edge: at that time, the Kutta condition implies the release of a trailing edge vortex in the opposite direction to the incident vortex; the trailing edge vortex then follows the incident vortex away from the airfoil, forming a “silent” vortex pair. A similar mechanism was found by Howe [32] and Guo [33], who considered the sound radiated by an incident vortex passing past stationary structures.

The present analysis is based on several approximations, listed along Sections 2 and 3. Perhaps the main approximation made is in not accounting for possible flow separation at the airfoil leading edge, and its effect on the acoustic radiation. Making use of potential-flow theory, we allow for a square-root singularity of the flow field at the leading edge, resulting in a finite leading edge suction force. As stated in Section 2, the same assumption has been made in previous theoretical studies of the flow generated around thin actuated structures, given that the amplitude of leading edge displacement is small [15–17]. Moreover, for the level of approximation applied in this work, any vorticity shed from the airfoil leading edge would convect over the airfoil surface, where its effects will be cancelled by image vortices in the airfoil, resulting in a silent source [2]. It is worthwhile to mention that existing experimental studies of the flow past thick plates (or plates having blunt leading edges) show that leading edge separation has an important impact on the outcome flow and acoustic fields (e.g., [34,35]). This effect, however, is beyond the scope of the present contribution.

The study has focused on a case where the airfoil is rigid and experiences simple harmonic motion. As noted in the Introduction, this simple forced-motion setup aims at complementing existing works studying vortex sound radiation in unforced and non-rigid (elastic) systems. The present scheme can be easily extended to consider the fluid-airfoil response to arbitrary (periodic or non-periodic) forcing of the structure, by taking the present analysis as a generalized Fourier component of the actual forcing signal. A less trivial extension of this work, taking account of the effect of airfoil elasticity, constitutes a topic of a study in progress.

## Acknowledgements

This work was supported by the Marie Curie International Reintegration, Grant no. PIRG-GA-2010-276837.

## References

- [1] R.D. Blevins, *Flow-Induced Vibration*, Van Nostrand Reinhold, New York, 1990 363 pp.
- [2] M.S. Howe, *Acoustics of Fluid–Structure Interactions*, Cambridge University Press, Cambridge, 1998 571 pp.
- [3] M.J. Shelley, J. Zhang, Flapping and bending bodies interacting with fluid flows, *Annual Review of Fluid Mechanics* 43 (2011) 449–465.
- [4] L. Huang, Mechanical modeling of palatal snoring, *Journal of the Acoustical Society of America* 97 (1995) 3642–3648.
- [5] T.M. Grundy, G.P. Keefe, M.V. Lowson, Effects of acoustic disturbances on low  $Re$  aerofoil flows, *Progress in Astronautics and Aeronautics* 195 (2001) 91–113.
- [6] M. Marcolini, E. Booth, H. Tadghighi, H. Hassan, C. Smith, L. Becker, Control of BVI noise using an active trailing edge flap, *Vertical Lift Aircraft Design Conference*, San Francisco, CA, 1995.
- [7] K. Nguyen, M. Betzina, C. Kitaplioglu, Full-scale demonstration of higher harmonic control for noise and vibration reduction on the XV-15 rotor, *American Helicopter Society 56th Annual Forum*, Virginia Beach, VA, 2000.
- [8] T. Maxworthy, The fluid dynamics of insect flight, *Annual Review of Fluid Mechanics* 13 (1981) 329–350.
- [9] H.C. Bennet-Clark, Acoustics of insect song, *Nature* 234 (1971) 255–259.
- [10] S. Drosopoulos, M.F. Claridge (Eds.), *Insect Sounds and Communication: Physiology, Behaviour, Ecology and Evolution*, Taylor and Francis, Boca Raton, FL, 2006. 532 pp.
- [11] L.J. Cator, B.J. Arthur, L.C. Harrington, R.R. Hoy, Harmonic convergence in the love songs of the dengue vector mosquito, *Science* 323 (2009) 1077–1079.
- [12] J. Sueur, E.J. Tuck, D. Robert, Sound radiation around a flying fly, *Journal of the Acoustical Society of America* 118 (2005) 530–538.
- [13] Y. Bae, Y.J. Moon, Aerodynamic sound generation of flapping wing, *Journal of the Acoustical Society of America* 124 (2008) 72–81.
- [14] A. Manela, M.S. Howe, On the stability and sound of an unforced flag, *Journal of Sound and Vibration* 321 (2009) 994–1006.
- [15] S. Alben, Optimal flexibility of a flapping appendage in an inviscid fluid, *Journal of Fluid Mechanics* 614 (2008) 355–380.

- [16] S. Michelin, S.G. Llewellyn Smith, Resonance and propulsion performance of a heaving flexible wing, *Physics of Fluids* 21 (2009) 071902.
- [17] A. Manela, Vibration and sound of an elastic wing actuated at its leading edge, *Journal of Sound and Vibration* 331 (2012) 638–650.
- [18] M.S. Howe, The influence of vortex shedding on the generation of sound by convected turbulence, *Journal of Fluid Mechanics* 76 (1976) 711–740.
- [19] M.S. Howe, The compact Green's function for a semi-infinite elastic plate, with application to trailing edge noise and blade-vortex interaction noise, *Journal of the Acoustical Society of America* 94 (1993) 2353–2364.
- [20] M.S. Howe, Elastic blade-vortex interaction noise, *Journal of Sound and Vibration* 177 (1994) 325–336.
- [21] A. Manela, M.S. Howe, The forced motion of a flag, *Journal of Fluid Mechanics* 635 (2009) 439–454.
- [22] A. Manela, Sound generated by a vortex convected past an elastic sheet, *Journal of Sound and Vibration* 330 (2011) 416–430.
- [23] H. Abou-Hussein, A. DeBenedictis, N. Harrison, M. Kim, M.A. Rodrigues, F. Zagadou, M.S. Howe, Vortex-surface interaction noise: a compendium of worked examples, *Journal of Sound and Vibration* 252 (2002) 883–918.
- [24] S.K. Tang, R.C.K. Leung, R.M.C. So, K.M. Lam, Acoustic radiation by vortex induced flexible wall vibration, *Journal of the Acoustical Society of America* 118 (2005) 2182–2189.
- [25] S.K. Tang, R.C.K. Leung, R.M.C. So, K.M. Lam, Vortex sound due to a flexible boundary backed by a cavity in a low Mach number mean flow, *Journal of the Acoustical Society of America* 121 (2007) 1345–1352.
- [26] S.K. Tang, Vortex sound in the presence of a low Mach number flow across a drum-like silencer, *Journal of the Acoustical Society of America* 129 (2011) 2830–2840.
- [27] M.S. Howe, *Theory of Vortex Sound*, Cambridge University Press, Cambridge, 2003 216 pp.
- [28] P. Saffman, *Vortex Dynamics*, Cambridge University Press, Cambridge, 1992 311 pp.
- [29] B. Thwaites, *Incompressible Aerodynamics: An Account of the Theory and Observation of the Steady Flow of Incompressible Fluid past Aerofoils, Wings, and Other Bodies*, Clarendon Press, Oxford, 1960 636 pp.
- [30] C.E. Brown, W.H. Michael, Effect of leading edge separation on the lift of a delta wing, *Journal of the Aeronautical Sciences* 21 (1954) 690–706.
- [31] C.E. Brown, W.H. Michael, On Slender Delta Wings with Leading-edge Separation, NACA Technical Note 3430, 1955.
- [32] M.S. Howe, Emendation of the Brown & Michael equation, with application to sound generation by vortex motion near a half-plane, *Journal of Fluid Mechanics* 329 (1996) 89–101.
- [33] Y.P. Guo, Application of the Ffowcs Williams/Hawkings equation to two-dimensional problems, *Journal of Fluid Mechanics* 403 (2000) 201–221.
- [34] M.C. Welsh, D.C. Gibson, Interaction of induced sound with flow past a square leading edged plate in a duct, *Journal of Sound and Vibration* 67 (1979) 501–511.
- [35] M.C. Welsh, A.N. Stokes, R. Parker, Flow-resonant sound interaction in a duct containing a plate. Part I: semi-circular leading edge, *Journal of Sound and Vibration* 95 (1984) 305–323.